

PRODUCTION OF THREE LARGE- p_{\perp} JETS IN HADRON-HADRON COLLISIONS

Z. KUNSZT* and E. PIETARINEN

Deutsches Elektronen-Synchrotron DESY, Hamburg, W. Germany

Received 28 June 1979
 (Final version received 28 August 1979)

We discuss physical effects given by QCD $2 \rightarrow 3$ scattering subprocesses. Transverse thrust distributions, jet and π^0 - π^0 azimuthal correlations, p_{out} distributions have been calculated at different energies with various cut-offs and are compared with the available data. Effects of transverse momentum smearing and jet broadening are also estimated. It is pointed out, that if the QCD description is correct, 3-jet effects will be revealed at transverse energies above $E_{\perp} \approx 20$ GeV and transverse jet momenta above $p_{\perp}^{\text{jet}} \approx 5$ GeV in future ISR, SPS $p\bar{p}$ collider and ISABELLE experiments.

1. Introduction

The study of large transverse momentum phenomena in hadron-hadron collisions was started by an ISR experiment in 1972 in which an anomalously large inclusive cross section has been found for inclusive production of large transverse momentum π^0 's as compared with the naive extrapolation from the low- p_{\perp} region [1]. It has provided some evidence that quark-quark scattering might be studied experimentally in the large transverse momentum region.

Motivated by the parton model, different hard scattering models have been developed which have all predicted production of transverse jets in hadron-hadron collisions [2–4].

In the naive parton model the large- p_{\perp} production of hadrons is described by the diagram in fig. 1. The large transverse momentum reaction is assumed to occur as a result of a single large-angle scattering of the constituents of the colliding hadrons followed by fragmentation of the final scattered constituent into the trigger hadron

$$E_c \frac{d^3\sigma}{d^3p_c} = \sum_{a,b,c,d} \int d^2q_{\perp a} \int d^2q_{\perp b} \int d^2q_{\perp c} \int \frac{dx_a}{\bar{x}_a} \int \frac{dx_b}{\bar{x}_b} x_a F_A^a(x_a, q_{\perp a}) \times F_B^b(x_b, q_{\perp b}) D_c^h(z_c, q_{\perp c}) \frac{1}{z_c} \frac{1}{\pi} \frac{d\hat{\sigma}^{ab \rightarrow cd}}{d\hat{t}}, \quad (1.1)$$

* Permanent address: Department of Atomic Physics, L. Eötvös University, Budapest, Hungary.

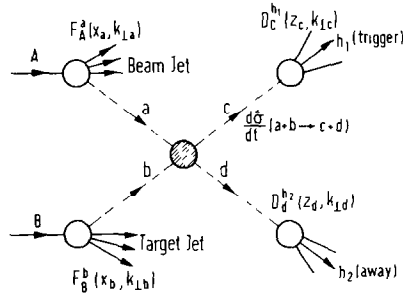


Fig. 1. Diagrammatic representation of the parton model description of large transverse momentum hadron production.

where $F_A^a(x_a, q_{\perp a})$ is the number of constituents of type a within a hadron A with momentum p_A ($k_a = x_a p_A + q_{\perp a}$, $p_A q_{\perp a} = 0$, $\bar{x}_a = (x_a^2 + q_{\perp a}^2/p_A^2)^{1/2}$) and $D_c^h(z_c, q_{\perp c})$ is the number of hadrons with momentum fraction z_c and transverse momentum $q_{\perp c} = p_c - z_c k_c$ ($q_{\perp c} \cdot k_c = 0$) coming from a given constituent of momentum k_c .

In the last years, however, a quantitative theory of strong interactions has emerged, quantum chromodynamics (QCD), which provides us with further theoretical ideas concerning formula (1.1) at least in four respects.

- (i) At relatively small distances the nature of the parton-parton scattering force

Table 1
Cross sections for the various $2 \rightarrow 2$ QCD scattering subprocesses

	$q\bar{q}' \rightarrow q\bar{q}'$ and $qq' \rightarrow qq'$	$qq \rightarrow qq$	$q\bar{q} \rightarrow q\bar{q}$	
$ A ^2$	$\frac{4}{9} \frac{\hat{s}^2 + \hat{u}^2}{\hat{t}^2}$	$\frac{4}{9} \left(\frac{\hat{s}^2 + \hat{u}^2}{\hat{t}^2} + \frac{\hat{s}^2 + \hat{t}^2}{\hat{u}^2} \right)$ $-\frac{8}{27} \frac{\hat{s}^2}{\hat{u}\hat{t}}$	$\frac{4}{9} \left(\frac{\hat{s}^2 + \hat{u}^2}{\hat{t}^2} + \frac{\hat{t}^2 + \hat{u}^2}{\hat{s}^2} \right)$ $-\frac{8}{27} \frac{\hat{u}^2}{\hat{s}\hat{t}}$	
	$q\bar{q} \rightarrow g\bar{g}$	$g\bar{g} \rightarrow q\bar{q}$	$q\bar{g} \rightarrow g\bar{q}$	$g\bar{g} \rightarrow g\bar{g}$
$ A ^2$	$\frac{32}{27} \left(\frac{\hat{u}^2 + \hat{t}^2}{\hat{u}\hat{t}} \right)$ $-\frac{8}{3} \left(\frac{\hat{u}^2 + \hat{t}^2}{\hat{s}^2} \right)$	$\frac{1}{6} \left(\frac{\hat{u}^2 + \hat{t}^2}{\hat{u}\hat{t}} \right)$ $-\frac{3}{8} \left(\frac{\hat{u}^2 + \hat{t}^2}{\hat{s}^2} \right)$	$-\frac{4}{9} \left(\frac{\hat{u}^2 + \hat{s}^2}{\hat{u}\hat{s}} \right)$ $+\frac{\hat{u}^2 + \hat{s}^2}{\hat{t}^2}$	$\frac{9}{2} \left(3 - \frac{\hat{u}\hat{t}}{\hat{s}^2} - \frac{\hat{u}\hat{s}}{\hat{t}^2} \right)$ $-\frac{\hat{s}\hat{t}}{\hat{u}^2}$

The differential cross section is given by $d\sigma/d\hat{t} = \pi\alpha_s^2(Q^2)/\hat{s}^2 |A|^2$.

denoted by $d\hat{\sigma}/d\hat{t}$ in eq. (1.1) is known [5]: it is given by the quasi-elastic scattering processes listed in table 1.

(ii) The QCD subprocesses must be corrected for the emission of gluons. It has recently been pointed out [6] that the infrared-divergent part of these corrections can be factorized into the running coupling constant of the subprocesses and into non-scaling quark, antiquark, gluon distributions and fragmentation functions, which are measured in deep inelastic lepton-hadron scattering and in e^+e^- annihilation.

(iii) Since quarks and gluons are confined in the transverse direction within the proton, the partons must have a ‘‘primordial’’ transverse momentum ≈ 300 MeV. In QCD, like in any renormalizable field theory, the transverse momenta within the bound state are not limited, in contrast with the assumption of the naive parton model approach. However, the large transverse momentum effects are calculable in QCD, because the effective coupling constant becomes small due to the asymptotic freedom and perturbation theory can be applied. These large momentum transfer processes give rise to a particular pattern of scale-breaking effects in electro- and neutrino production which is confirmed in recent high-precision experiments [7].

Large transverse momentum effects are also revealed by the transverse momentum distribution of the lepton pairs [8–13] or heavy quarkonia [14] produced in hadron-hadron collisions. In particular, the p_{\perp} spectrum of the $\mu^+\mu^-$ pair (both off and on resonance) is predicted to have a non-gaussian large- p_{\perp} tail, which becomes flatter as the energy and/or the mass of the lepton pair is increased in agreement with the measurements [15,16].

Similarly the large momentum tail of the p_{out} spectrum in two-particle correlations measured at ISR [17] is expected to be dominated by the contributions of the $2 \rightarrow 3$ subprocesses [4,18].

(iv) Finally, QCD implies the existence of three or more jet events. A great deal of activity has been devoted to this question in the last year. Various infrared-finite observables have been proposed to describe event structures, calculable in QCD. Obviously e^+e^- annihilation into hadrons is the cleanest place to study QCD 3-jet effects: there is only one energy scale, the non-perturbative mechanism occurs only in the final state (in the case of inclusive treatment it becomes unimportant). The first experimental attempt to study 3-jet configurations has recently been carried out on the Υ resonance by the PLUTO group [19]. The study of the production of 3 large transverse momentum jets in hadron collisions is expected to be feasible, as well. The most important question is, of course, how much of the QCD effects can be revealed from the non-perturbative background.

Large- p_{\perp} meson production has been studied within the QCD framework by various authors [20–25]. The most exhaustive study has been performed by Feynman, Field and Fox [21] (FFF). They have pointed out that the QCD description may explain the apparent p_{\perp}^{-8} behaviour of the inclusive cross sections, despite the p_{\perp}^{-4} behaviour of the hard scattering processes if we bring in all the essential ingredients of QCD: gluon scattering contributions in addition to scattering of quarks,

scale breaking effects in the wave functions and large transverse momentum smearing. However, several problems have remained. The transverse momentum smearing required for large- p_{\perp} events appears to be too large, the average value of p_{out} is higher than the predicted one, the description of charm production is still quite controversial, etc.

We remind the reader that all the analyses performed so far are based solely on the $2 \rightarrow 2$ subprocesses ^{*} (see table 1). We may argue that in the present range of energies, $\alpha_s(Q^2)$ is not sufficiently small to make the lowest-order approximation as precise as needed. Higher-order radiative corrections may become important. In particular one may hope that the problems encountered above can be remedied, at least partly, by adding to the Born diagrams the first-order QCD corrections. These corrections to single particle distributions of the large transverse momentum jet and/or meson production consist of the contributions of the $2 \rightarrow 3$ subprocesses and loop corrections. Therefore, essential cancellations may occur and the whole infrared-ultraviolet renormalization procedure has to be performed. Such a complete study has been carried out only for the Drell-Yan process [27,28]. There are, however, several physical quantities like the p_{\perp} distribution of heavy quarkonia produced in hadron-hadron collisions, 3-jet production, azimuthal angle correlations of large transverse momentum particles, p_{out} distributions, transverse thrust distributions etc., for which the Born approximations are given by the $2 \rightarrow 3$ subprocesses. The contributions of the $2 \rightarrow 2$ subprocesses, and therefore also the first-order loop corrections, vanish due to kinematical reasons.

Our main aim is to present a realistic phenomenological calculation of 3-jet contributions relevant for the presently available data obtained at ISR. In particular, p_{out} distributions, jet and $\pi^0\pi^0$ azimuthal correlations and transverse thrust distributions have been calculated at different energies with various cut-off conditions and are compared with the data. We include all the important ingredients, namely 4q-1g, 2q-3g contributions, q^2 dependent parton distribution functions, jet fragmentation and p_{\perp} smearing. The contributions of the 5-gluon amplitudes at ISR energies with $p_{\perp} > 3$ GeV/c give only small corrections. This is expected since the contribution of gluon-gluon elastic scattering to the large- p_{\perp} spectrum of inclusively produced mesons in proton-proton collisions is negligible even with the use of relatively flat gluon wave functions. The radiative corrections given by the subprocess $gg \rightarrow ggg$ are negligible for the same reason. They are suppressed by folding with the steeply falling gluon wave functions. We remark that the calculation of this contribution is particularly ambiguous, since just the gluon wave function and the fragmentation of the gluon jets are the most uncertain unknown quantities of the QCD model.

^{*} The possible effects of the $2 \rightarrow 3$ subprocesses have been taken into account only in the transverse momentum smearing, assuming a larger value for $\langle k_{\perp} \rangle$ ($\langle k_{\perp} \rangle \approx 900$ MeV). An attempt to explain the $\pi^0\pi^0$ azimuthal angle correlation data by use of the subprocess $qq \rightarrow gqq$ has been made by Kripfganz and Schiller [26].

In sect. 2 the calculation of the parton cross sections is described and some of their essential features are discussed. In sect. 3 we specify our parton wave functions and decay functions. Present ambiguities given by Q^2 dependent parton distributions and fragmentation functions, running coupling constant, smearing at low p_{\perp} , cut-off dependence, etc., are also investigated here. In sect. 4 we present and discuss the results, sect. 5 is the conclusion and in the appendix we give the formula for the cross section of the process $qq' \rightarrow qq'g$.

2. Calculation of the parton cross sections

The $2 \rightarrow 3$ QCD scattering subprocesses can be classified into four classes (see table 2), namely to $2q$ - $2q$ - $1g$ (the quark pairs have different flavours); $4q$ - $1g$ (the quarks have the same flavour) $2q$ - $3g$ and $5g$ processes [29].

The invariant amplitude squares have to be calculated for each class. The cross sections within a given class are simply related by crossing symmetry. The Feynman diagrams giving the amplitudes for the processes of each of the four classes are shown in fig. 2.

To leading order in perturbative QCD, the differential cross section for all $2 \rightarrow 3$ subprocesses (with massless partons)

$$a_4(-k_4) + a_5(-k_5) \rightarrow a_1(k_1) + a_2(k_2) + a_3(k_3) \quad (2.1)$$

can be given as

$$\frac{d^4\sigma}{dq^2 dt ds d\Omega^{\text{TY}}} = C \frac{\alpha_s^3}{8\pi s^2} W[\{s_{ij}\}], \quad (2.2)$$

where C denotes color and spin averaging factor, α_s is the QCD running coupling constant, q^2 , t , s , s_{ij} denote invariant variables

$$q = k_1 + k_2, \quad t = (k_4 + q)^2, \quad s = (k_4 + k_5)^2, \quad (2.3a)$$

$$s_{ij} = (k_i + k_j)^2. \quad (2.3b)$$

Ω^{TY} denotes the Treiman-Yang solid angles (see fig. 3), defined in the frame $\mathbf{q} = 0$

Table 2
Four subclasses of crossing related $2 \rightarrow 3$ subprocesses

$qq'qq'g$	$qqqqg$	$qqggg$	$ggggg$
$qq' \rightarrow qq'g$	$qq \rightarrow qqg$	$gq \rightarrow gqg$	$qq \rightarrow ggg$
$q\bar{q}' \rightarrow q\bar{q}'g$	$q\bar{q} \rightarrow q\bar{q}g$	$q\bar{q} \rightarrow ggg$	
$q\bar{q}' \rightarrow q'\bar{q}'g$	$gq \rightarrow q\bar{q}q$	$gg \rightarrow gq\bar{q}$	
$gq \rightarrow q\bar{q}'q'$			

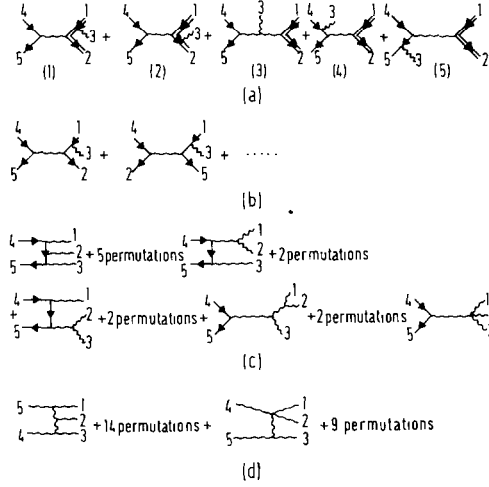


Fig. 2. Lowest-order QCD contributions to the production of three large transverse momentum jets in hadron-hadron collisions. There are (a) 5 diagrams for the amplitudes $q\bar{q}q'\bar{q}'g$, (b) 10 diagrams for $q\bar{q}q\bar{q}g$; (c) the amplitude of $ggq\bar{q}$ is described by 16 diagrams, (d) the 5-gluon amplitude is given by 25 diagrams.

with the relations

$$\cos \theta^{\text{TY}} = - \left. \frac{\mathbf{k}_2 \cdot \mathbf{k}_5}{|\mathbf{k}_2| \cdot |\mathbf{k}_5|} \right|_{q=0}, \quad \cos \phi^{\text{TY}} = - \left. \frac{(\mathbf{k}_2 \times \mathbf{k}_5) \cdot (\mathbf{k}_3 \times \mathbf{k}_5)}{|\mathbf{k}_2 \times \mathbf{k}_5| \cdot |\mathbf{k}_3 \times \mathbf{k}_5|} \right|_{q=0}. \quad (2.4)$$

The function $W[\{s_{ij}\}]$ is the invariant matrix element squared for the problem. For each class of the subprocess given in table 2 we can write the corresponding invariant function as a trace of two real symmetric matrices

$$W^{(F)}[\{s_{ij}\}] = \sum_{i,j=1}^{N_F} C_{ij}^F A_{ij}^F[\{s_{ij}\}], \quad (2.5)$$

where F can take values a, b, c, d corresponding to the different classes (table 2) and diagrams (fig. 2), N_F gives the number of the Feynman diagrams ($N_a = 5$, $N_b = 10$,

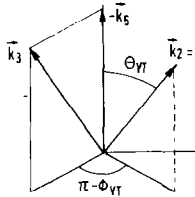


Fig. 3. Definition of the Treiman-Yang angles.

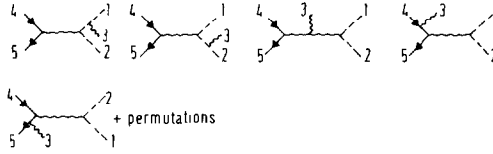


Fig. 4. Ghost diagrams contributing to the 3g-2q amplitude.

$N_c = 16$ and $N_d = 25$) and C_{ij} are the matrices of the color factors. The matrix elements $A_{ij}^F[\{s_{ij}\}]$ are given by the equation

$$A_{ij}^F = \sum_{\substack{\text{initial, final} \\ \text{spin}}} T_i^F T_j^{F*}, \quad (2.6)$$

where the T_i^F 's denote the Lorentz part of the amplitudes defined by the Feynman diagrams of fig. 2. We have performed the calculation of the matrix elements A_{ij}^F for the first three subclasses a, b, c with the help of the computer program REDUCE^{*}. In the appendix we give explicitly the matrices $A_{ij}^{(a)}$ and $C_{ij}^{(a)}$, for the 2q-2q-1g subprocess, where the crossing procedure is also illustrated. The expressions obtained for $C_{ij}^{(b)}$, $A_{ij}^{(b)}$ (4q-1g) and $C_{ij}^{(c)}$, $A_{ij}^{(c)}$ (2q-3g) are exceedingly longer than the formula given in the appendix for $C_{ij}^{(a)}$, $A_{ij}^{(a)}$, since if the number of the external gluon lines is increased, we have more Feynman diagrams and more 3- and/or 4-gluon vertices. Furthermore, if we calculate in the Feynman gauge, a large number of ghost diagrams to be added (see fig. 4); in the physical gauge, however, we have a longer expression for the gluon helicity sums:

$$\sum_{\lambda} \epsilon_{\mu}(\lambda) \epsilon_{\nu}^*(\lambda) = -g_{\mu\nu} + \frac{n_{\mu}k_{\nu} + n_{\nu}k_{\mu}}{nk} - \frac{k_{\mu}k_{\nu}}{(nk)^2}, \quad (2.7)$$

where n is an arbitrary timelike unit vector ($n^2 = 1$). The algebraic calculation of A_{ij}^F has been performed in the Feynman gauge which has been checked with an entirely numerical calculation performed in the physical gauge. In order to understand better the basic properties of the pointlike, QCD partonic cross sections of the $2 \rightarrow 3$ subprocesses, we have calculated integrated (unphysical) cross-section values without folding them with structure and fragmentation functions. To avoid contributions from infrared and mass singularities, we applied transverse momentum, polar angle and acoplanarity angle cuts. The transverse momenta and polar angles are defined for c.m. collisions with respect to the beam directions

$$\theta_i = \arccos\left(\frac{\mathbf{p}_{\text{beam}} \cdot \mathbf{p}_i}{|\mathbf{p}_{\text{beam}}| \cdot |\mathbf{p}_i|}\right), \quad (2.8)$$

where \mathbf{p}_i denotes the three-momentum of the parton i in the final state. The ac-

^{*} The contribution of the 5-gluon amplitudes, relevant at higher energies, will be discussed elsewhere [30].

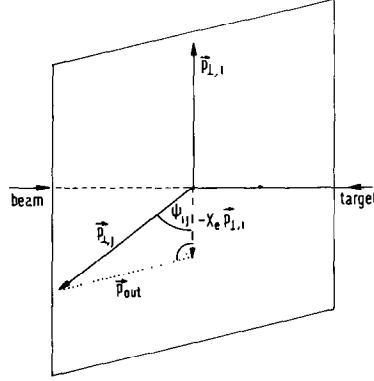


Fig. 5. Definition of the kinematical variables p_{out} , acoplanarity angle ψ , transverse momenta $p_{\perp i}$ and x_e .

planarity angle is defined as the angle of two planes defined by the vector pairs $(\mathbf{p}_{beam}, \mathbf{p}_i)$, $(\mathbf{p}_{beam}, \mathbf{p}_j)$, $i \neq j$ (see fig. 5) ^{*}, i.e.,

$$\psi_{ij} = -\arccos \left[\frac{(\mathbf{p}_b \times \mathbf{p}_i) \cdot (\mathbf{p}_b \times \mathbf{p}_j)}{|\mathbf{p}_b \times \mathbf{p}_i| \cdot |\mathbf{p}_b \times \mathbf{p}_j|} \right]. \quad (2.9a)$$

The azimuthal angle difference between the transverse momenta of $\mathbf{p}_{\perp i}$, $\mathbf{p}_{\perp j}$ of the partons i and j , respectively, is simply given as

$$\phi_{ij} = \pi - \psi_{ij}. \quad (2.9b)$$

In table 3, we give some integrated parton cross-section values for $2 \rightarrow 3$ subprocesses and (in parentheses) for $2 \rightarrow 2$ subprocesses. We assumed that only two (i, j) out of the three final particles are observed. In other words, we applied cuts only for the three-momenta of two final partons. The cross-section values have been calculated at total c.m. energy $\sqrt{s} = 20$ GeV, with polar angle cuts $\theta_c = 15^\circ, 30^\circ, 45^\circ, 60^\circ$ both for the $2 \rightarrow 2$ and $2 \rightarrow 3$ processes. In case of the $2 \rightarrow 3$ scatterings, in addition we used transverse momentum cuts $p_{\perp i}, p_{\perp j} > 2.5$ GeV/ c and acoplanarity cuts $\psi_c = \frac{1}{8}\pi, \frac{1}{4}\pi$

$$180^\circ - \psi_c \geq \psi_{ij} \geq \psi_c. \quad (2.10)$$

The transverse momentum cut is needed to avoid soft infrared singularities, the acoplanarity cut ensures that we have 3-jet-like configurations. These cuts are not symmetric in the momenta of the final particles. Table 3 gives the averaged value of the three possible pairings of the final “particles” as “observed particles”. The

^{*} The same definition is used in the study of hard photon bremsstrahlung in QED, e.g., in Bhabha scattering [31].

Table 3
 Cross-section values in nanobarns for seven different $2 \rightarrow 3$ scattering subprocesses, with polar angle, azimuthal angle and p_{\perp} cuts, $\theta_c, \phi_c, p_{\perp c}$ at incoming energy $\sqrt{s} = 20$ GeV

$qq' \rightarrow qq'g$ (nb)	$qq' \rightarrow q\bar{q}g$ (nb)	$q\bar{q} \rightarrow q\bar{q}g$ (nb)	$gq \rightarrow q\bar{q}q$ (nb)	$gq \rightarrow g\bar{q}q$ (nb)	$gg \rightarrow gq\bar{q}$ (nb)	$qq \rightarrow ggg$ (nb)	θ_c	Comments
4500 (1.4×10^4)	4600 (1.4×10^4)	32 (53)	107	1.2×10^4 (3.2×10^4)	530 (200)	150 (700)	15°	$\phi_c = \frac{1}{8}\pi$
1200 (2000)	1240 (2000)	20 (41)	38	3000 (4800)	180 (70)	85 (255)	30°	$p_{\perp i} > 2.5$ GeV/c
300 (630)	343 (630)	11 (29)	13	830 (1600)	65 (32)	41 (115)	45°	
75 (250)	91 (250)	4.6 (18)	0.93	240 (500)	21 (15)	15 (54)	60°	
1400 (1.4×10^4)	1500 (1.4×10^4)	15 (53)	41	3800 (3.2×10^4)	200 (200)	158 (700)	15°	$\phi_c = \frac{1}{4}\pi$
450 (2000)	500 (2000)	9.2 (41)	16	1200 (4800)	80 (70)	35 (255)	30°	$p_{\perp i} > 2.5$ GeV/c
32 (630)	41 (630)	4.8 (29)	5.6	350 (1600)	27 (32)	17 (115)	45°	
5.5 (250)	7.6 (250)	2.0 (18)	1.8	100 (500)	7.9 (15)	6.6 (54)	60°	

The numbers in parentheses are the values of the cross sections for the corresponding $2 \rightarrow 2$ processes with the same value of θ_c .

phase-space integrations were made by a Monte Carlo method and the numbers have 5–10% accuracy. The cross sections with equal flavour are not given, since they differ from the ones with ($q \neq q'$) only about 5–10%.

We used running coupling constant defined as follows:

$$\alpha_s(Q^2) = \frac{12\pi}{(33 - 2N_F) \ln(Q^2/\Lambda^2)} . \quad (2.11)$$

With $\Lambda = 0.5$ GeV, $N_F = 5$, for the Q -value we have chosen the transverse energy

$$E_{\perp}^{2 \rightarrow 3} = |\mathbf{p}_{1\perp}| + |\mathbf{p}_{2\perp}| + |\mathbf{p}_{3\perp}| . \quad (2.12)$$

What is the correct quantity to use for Q^2 in the case of the $2 \rightarrow 2$ or $2 \rightarrow 3$ subprocesses, contributing to 2-jet and 3-jet production in pp collisions, is not clear at present. Our Q value is factor 2–2.5 larger than the one used by Feynman et al. [21]. For the $2 \rightarrow 2$ subprocesses we take similarly

$$E_{\perp}^{2 \rightarrow 2} = |\mathbf{p}_{1\perp}| + |\mathbf{p}_{2\perp}| = 2|\mathbf{p}_{1\perp}| . \quad (2.13)$$

These ambiguities are not important if we study the relative rates of 3-jet–2-jet contributions, but changing Λ by such an amount can change the normalization of the cross sections by 20–30%.

As we can see from table 3 the relative magnitude of the hard gluon bremsstrahlung cross sections with respect to the Born cross section can be enhanced or suppressed by changing the magnitude of the cuts: e.g., changing the value of ψ_c from $\frac{1}{8}\pi$ to $\frac{1}{4}\pi$ or the value of p_{\perp}^c from 2.5 to 5 GeV, the hard gluon cross sections become smaller by a factor ≈ 3 , on average. The critical value of ψ_c and p_{\perp}^c where radiative corrections become exceedingly large (30–40%) may be interpreted as a measure of “jet broadening” of the jets produced in hadron-hadron collisions. This is further illustrated by fig. 6, where cross sections of three different hard scattering processes ($qq \rightarrow q\bar{q}g$, $gq \rightarrow ggq$ and $gg \rightarrow gq\bar{q}$) are plotted as functions of ϵ and δ . The cross-section value of the corresponding elastic scattering is also indicated. Here δ and ϵ denote angle and energy fraction cuts, respectively, similar to the ones proposed by Serman and Weinberg [32]: in our definition all the angles between the three-momenta of the final particles and the *beam* direction are required to be larger than δ and the energy fraction carried by any of the final jets is required to be larger than ϵ .

It is obvious from table 3 and fig. 6 that, in general, the hard gluon emission processes give 20–30% effects with $\sigma = 0.2$, $\delta = 0.1$ –0.2 as compared with the leading-order cross sections, similarly to jets produced in e^+e^- annihilation. There is, however, a very interesting exception: $gg \rightarrow gq\bar{q}$. In this case the relative magnitude of the cross section with respect to the Born cross section is 5–6 times larger than the same ratio for all the other processes in table 3. This exceptional value of the hard gluon corrections, however, has a very simple explanation. As it can be seen from table 1, the cross-section ratio

$$\sigma(gg \rightarrow gg)/\sigma(gg \rightarrow q\bar{q}) \approx 150\text{--}250 \quad (2.14)$$

the relative importance of the different subprocesses and the ratio $\sigma(3\text{-jet})/\sigma(2\text{-jet})$ generally remained almost the same (see table 3 and fig. 6). This also indicates that if factorization of the collinear and infrared singularities holds for transverse momentum distributions, as well, then instead of p_{\perp} we must use the dimensionless variable [34] $x_{\perp} = 2p_{\perp}/\sqrt{s}$.

We also have studied the acoplanarity distributions of the subprocesses, which turned out to be qualitatively similar to the corresponding QED distributions. We mention finally that changing the colour factors to the QED values, we could reproduce the acoplanarity distributions, e.g., for Bhabha scattering, published in table 6 of ref. [31].

3. Parton distribution functions, physical cross sections

3.1. Parton wave functions

According to formula (1.1), in the QCD approach, physical cross sections are obtained by folding the parton cross sections with parton wave functions and decay functions, which are measured in deep inelastic leptonproduction and in e^+e^- annihilation. However, the distributions of gluons within the proton, $F_h^g(x, Q_0^2)$, and the distribution of hadrons in a gluon jet, $D_g^h(z, Q_0^2)$, at some reference momenta are very weakly constrained by the deep inelastic leptonproduction data. In the analysis of the hadron-hadron scattering data they are chosen in such a way as to provide a qualitatively good description of the experimental features of high- p_{\perp} processes, namely large transverse momentum meson production, p_{\perp} distribution of lepton-pair production, p_{\perp} distribution of heavy quarkonium production, etc. The data still have various ambiguities, so presently we have quite a lot of freedom in the choice for $F_h^g(x, Q_0^2)$ and $D_g^h(z, Q_0^2)$. These ambiguities, however, become less important in making a comparison of the two- and three-jet production rates.

In our analysis we have chosen two types of distribution which yield approximate upper and lower estimates of the ambiguities present in the gluon content of the proton.

(i) As a first set of distributions we have used the parton distributions of Buras and Gaemers [35] with scaling deviation as predicted by QCD, where the input densities at $Q^2 = Q_0^2 = 1.8$ have been obtained from fits to deep inelastic leptonproduction data. In particular for the valence-quark distribution we used their simple parametrization of the QCD predicted Q^2 dependence, whereas for the sea and gluon distributions we used the improved Q^2 dependent wave function as calculated by Owens and Reya [36] by Mellin inverting the first 100 moments given by QCD and fitting the result with simple analytic expressions. More explicitly, the input values have been fixed by the experimental values of the lowest moments at $Q_0^2 = 1.8$. Using the definition $u = u_v + \xi$, $d = d_v + \xi$, $\bar{u} = \bar{d} = s = \bar{s} = \xi$,

$$\langle xu_v(Q_0^2) + xd_v(Q_0^2) \rangle_1 = 0.488, \quad (3.1a)$$

$$\langle x\xi(Q_0^2) \rangle_1 = 0.0183, \quad (3.1b)$$

$$\langle xG(Q_0^2) \rangle_1 = 0.402, \quad (3.1c)$$

where the moments are defined by

$$M_i(n, Q^2) = \langle F_i(x, Q^2) \rangle_n = \int_0^1 dx x^{n-1} F_i(x, Q^2). \quad (3.2)$$

The full Q^2 dependence for the valence part is chosen to be the same as that given by the parametrization of Buras and Gaemers by fitting the first 12 moments predicted by QCD,

$$xu_v(x, Q^2) + xd_v(x, Q^2) = \frac{3}{B(\eta_1, 1 + \eta_1)} x^{\eta_1} (1-x)^{\eta_2}, \quad (3.3a)$$

$$xd_v(x, Q^2) = \frac{1}{B(\eta_3, 1 + \eta_4)} x^{\eta_3} (1-x)^{\eta_4}, \quad (3.3b)$$

with

$$\eta_1 = 0.70 - 0.176 \bar{s}, \quad \eta_2 = 26 + 0.80 \bar{s}, \quad (3.3c)$$

$$\eta_3 = 0.85 - 0.24 \bar{s}, \quad \eta_4 = 3.35 + 0.816 \bar{s}, \quad (3.3d)$$

where $\bar{s} = \ln[\ln(Q^2/\Lambda^2)/\ln(Q_0^2/\Lambda^2)]$, $Q_0^2 = 1.8 \text{ GeV}^2$. The use of the Euler beta function, $B(\eta_i, 1 + \eta_i)$, $i = 1, 3$ ensures baryon-number conservation for all values of Q^2 .

The x -dependence of the sea and gluon distributions has been chosen to be in agreement with naive counting rules

$$x\xi(x, Q_0^2) = 0.147(1-x)^7, \quad xG(x, Q_0^2) = 2.4(1-x)^5. \quad (3.4)$$

For their Q^2 dependence, we adopted the results of Owens and Reya (see eqs. (3)–(7) and table 1 in ref. [36]).

(ii) Some of the physical correlations have also been calculated with Q^2 independent wave functions and with the gluon wave functions proposed by FFF [21]

$$xG(x, Q_0^2 = 4 (\text{GeV}/c)^2) = 0.80 (1 + 9x)(1-x)^4. \quad (3.5)$$

In certain cases we have also included transverse momentum smearing with gaussian smearing functions $\sim e^{-k_{\perp}^2/2\sigma}$.

3.2. Decay functions

In most of the calculations for the results presented in sect. 4, we use a simple parametrization of the effective fragmentation functions which represents a reasonably good analytic approximation for the description of the data of inclusive meson production in e^+e^- annihilation and lepton-hadron interactions [37].

For completeness we list the naive fragmentation functions used in the calculation of the π^0 - π^0 azimuthal correlation and p_{out} distributions (see figs. 10 and 12).

Following refs. [37,38] we parametrize the independent fragmentation functions as follows:

$$\begin{aligned} zD_{\text{u}}^{\pi^+} &= a\sqrt{z}(c-z) + \xi_{\pi}(1-z)^2, & zD_{\text{u}}^{\pi^-} &= \xi_{\pi}(1-z)^2, \\ zD_{\text{u}}^{\text{K}^+} &= b\sqrt{z}(c-z) + \xi_{\text{K}}(1-z)^2, & zD_{\text{u}}^{\text{K}^-} &= \xi_{\text{K}}(1-z)^2, \\ zD_{\text{s}}^{\text{K}^-} &= a\sqrt{z}(c-z) + \xi_{\text{K}}(1-z)^2, \end{aligned} \quad (3.6)$$

where the limiting behaviour

$$D_{\text{s}}^{\text{K}^-}/D_{\text{u}}^{\pi^+} \rightarrow 1, \quad \text{as } z \rightarrow 1, \quad D_{\text{u}}^{\text{K}^+}/D_{\text{s}}^{\text{K}^-} \rightarrow 1, \quad \text{as } z \rightarrow 0$$

has also been required.

Two of the coefficients can be eliminated by satisfying the energy and isospin sum rules

$$\int dz \sum z D_{\text{q}}^{\text{h}}(z) = 1, \quad (3.7a)$$

$$\int dz [(D_{\text{u}}^{\pi^+} - D_{\text{u}}^{\pi^-}) + \frac{1}{2}(D_{\text{u}}^{\text{K}^+} - D_{\text{u}}^{\text{K}^0}) + \frac{1}{2}(D_{\text{u}}^{\text{K}^0} - D_{\text{u}}^{\text{K}^-})] = \frac{1}{2}. \quad (3.7b)$$

We assume [37], as indicated by the data, SU(3) breaking $\xi_{\text{K}}/\xi_{\pi} = \frac{1}{2}$ and

$$(a+b)(c-1) \approx 0.075$$

given by the production of charged hadrons in deep inelastic neutrino scattering, so we have

$$a = 0.225, \quad b = \frac{1}{2}a, \quad c = 1.222, \quad \xi_{\pi} = 0.488. \quad (3.8)$$

With these parameters there is a small leakage of quark charge due to SU(3) breaking.

Choosing the gluon decay functions one can be guided by the following arguments [37]: on one hand, the energy sum rule has to be satisfied:

$$\int dz z(3D_{\text{g}}^{\pi} + 4D_{\text{g}}^{\text{K}}) = 1;$$

furthermore in QCD, where $q\bar{q}$ pairs are produced *via* gluons emitted by the initial quark, the gluon fragmentation function $D_{\text{g}}^{\text{h}}(z)$ must be steeper than the favoured and flatter than the unfavoured quark distribution as $z \rightarrow 1$. So it appears reasonable to assume

$$zD_{\text{g}}^{\text{h}} = c^{\text{h}}(1-z)^{1.5}. \quad (3.9)$$

Assuming again 50% SU(3) breaking $c^{\pi}/c^{\text{K}} \approx 2$ we obtain $c^{\pi} = \frac{1}{2}$, $c^{\text{K}} = \frac{1}{4}$. We remark that FFF assumed at $Q_0^2 = 4 \text{ GeV}^2$ the form

$$zD_{\text{g}}^{\pi^0} = 0.48(1-z)^2. \quad (3.10)$$

In order to understand the possible mechanism producing the ‘‘same side’’ enhancement in the azimuthal angle correlation data (see fig. 10) we have also used the Feynman and Field [4] Monte Carlo jet development model for the contributions of the $2 \rightarrow 2$ subprocesses. In the case of the 3-jet contributions we have also assumed factorizable gaussian transverse momentum distributions for the π^0 fragmentation. We did not include the Q^2 dependence (as predicted by QCD) for the fragmentation function * .

3.3. Physical cross sections

The differential cross section of 3-jet production can be given in the form [see eq. (1.1)]

$$E_c E_d E_e \frac{d^9 \sigma^{AB \rightarrow cde}}{d^3 k_c d^3 k_d d^3 k_e} = \sum_{a,b} \int \frac{dx_a}{x_a} \frac{dx_b}{x_b} d^2 \mathbf{q}_{\perp a} d^2 \mathbf{q}_{\perp b} \bar{x}_a F_A^a(x_a, Q^2, \mathbf{q}_{\perp a}) \quad (3.11)$$

$$\times \bar{x}_b F_B^b(x_b, Q^2, \mathbf{q}_{\perp b}) \frac{8\delta}{\pi} \frac{d^4 \hat{\sigma}^{ab \rightarrow cde}(s_{ij})}{d|t| dq^2 d\Omega^{TY}} \delta^4(k_a + k_b - k_c - k_d - k_e),$$

where the parton cross section $d^4 \hat{\sigma}$ is given in eq. (2.2). We have studied acoplanarity angle, p_{out} and transverse thrust distributions. The transverse thrust [39] is defined by

$$T_{\perp} = 2 \frac{\max_i \sum_j (|\mathbf{k}_{\perp j} \cdot \mathbf{n}|)}{E_{\perp}}, \quad (3.12)$$

where \sum denotes sum over all particles in one semicircle, \mathbf{n} is a unit vector in the transverse momentum plane which has to be chosen to maximize T_{\perp} and E_{\perp} is the transverse energy [see eq. (2.13)]

$$E_{\perp} = \sum_{i=c,d,e} |\mathbf{k}_{\perp i}|. \quad (3.13)$$

The differential cross section at fixed E_{\perp} can be written as

$$\frac{d^2 \sigma^{(3\text{-jet})}}{dE_{\perp} dT_{\perp}} = \sum_{c,d,e} \int \dots \int \frac{d^9 \sigma^{AB \rightarrow cde}}{d^3 k_c d^3 k_d d^3 k_e} d^3 k_c d^3 k_d d^3 k_e \quad (3.14)$$

$$\times \delta(T_{\perp} - 2 \max_j (k_j/E_{\perp})) \delta(E_{\perp} - \sum_{j=i}^e |\mathbf{k}_{\perp j}|).$$

The acoplanarity (or azimuthal) distributions are given by similar expressions.

* It would further suppress the subprocesses where gluons are produced in the final states. However, for the applications presented in this paper this effect is not important.

Two or more particle correlations can be obtained from the 3-jet cross sections (3.11) by folding it with the parton decay functions:

$$\begin{aligned}
 E_{h_1} E_{h_2} \frac{d^6 \sigma^{h_1 h_2}}{d^3 p_{h_1} d^3 p_{h_2}} &= \sum_{j,k,l} \int \dots \int dz_j dz_k d^2 \mathbf{q}_{\perp j} d^2 \mathbf{q}_{\perp k} \\
 &\times \frac{d^9 \sigma^{AB \rightarrow j+k+l}}{d^3 k_j d^3 k_k d^3 k_l} E_j E_k E_l \bar{z}_j D_j^{h_1}(z_j, Q^2, \mathbf{q}_{ij}) \\
 &\times \bar{z}_k D_k^{h_2}(z_k, Q^2, \mathbf{q}_{\perp k}) \frac{1}{z_j^3 z_k^3}, \quad (3.15)
 \end{aligned}$$

where $\mathbf{q}_{\perp j} = \mathbf{p}_{h_1} - z_j \mathbf{k}_j$ and $\bar{z}_j = (z_j^2 + \mathbf{q}_{\perp j}^2 / k_j^2)^{1/2}$. Azimuthal correlations of two neutral pions $d^2 \sigma^{\pi^0 \pi^0} / dE_{\perp} d\psi$ and p_{out} distributions $d^2 \sigma^{\pi^0 \pi^0} / dE_{\perp} dp_{\text{out}}$ are defined by analogous formulae. We remind the reader that p_{out} is defined [1] as (see fig. 5)

$$p_{i \text{ out}} = \left| \frac{[\mathbf{p}_{\text{beam}} \times \mathbf{p}_{\perp \text{ trigger}}]}{|\mathbf{p}_{\text{beam}}| |\mathbf{p}_{\perp \text{ trigger}}|} \cdot \mathbf{p}_i \right|. \quad (3.16)$$

Various infrared-finite observables have been proposed in the literature for the analysis of event shapes of multijet events. Obviously all of them can be generalized to the study of the three-jet production in hadron-hadron collisions, putting the vector for the transverse energy flow as a function of the azimuthal angle [40], ‘‘higher’’ transverse thrust variables, rotationally invariant C_i variables of Fox and Wolfram [41]

$$C_i = \left| \sum_j |\mathbf{p}_{\perp j}| e^{i l \phi_j} \right|^2, \quad (3.17)$$

where the $p_{\perp i}$ ’s are the perpendicular momenta of the resulting hadrons and ϕ_i is measured relative to an arbitrary axis chosen in the plane of transverse momenta, etc. However, with the meagre data available at present, we feel that it is premature to work out distributions for all these variables.

One may try to study 3-particle correlations as well, although the rate will be very small.

3.4. Smearing and cuts

In the presently accessible energy and transverse momentum range it is expected that almost all of the three-jet effects are below the ‘‘noise’’ of the smeared two-jet contributions.

In order to obtain a rough estimate of the relative magnitude of the 2-jet and 3-jet contributions to the transverse thrust distribution we used a crude approximation: the primordial transverse momenta of the partons (inside the bound-state wave function) and the hadrons (inside jets) have been neglected; however, we

smear the 2-jet cross section with some “reasonable width”. In particular it has been estimated [40,42] that the transverse thrust distribution of the 2-jet contribution has an approximate gaussian shape with some effective “non-perturbative” width

$$(\Delta T_1)_{\text{NP}} \simeq \frac{1}{2} n(E_{\perp}) \frac{\langle p_{\perp} \rangle}{E_{\perp}}, \quad \langle p_{\perp} \rangle = 300 \text{ MeV}, \quad (3.18)$$

with multiplicity

$$n(E_{\perp}) = 1.0 + 2.1 \ln E_{\perp}^2. \quad (3.19)$$

So the normalized transverse thrust distribution (which is expected to vanish at $T = 1$) has the form

$$\frac{1}{d\sigma/dE_{\perp}} \frac{d^2\sigma}{dT_{\perp} dE_{\perp}} = \frac{2}{(\Delta T)_{\text{NP}}^2} e^{-(1-T)^2/(\Delta T)_{\text{NP}}^2} (1-T) = F_s(T), \quad (3.20)$$

(where $E_{\perp} = 2p_{\perp}^{\text{jet}}$ for 2-jet production). Obviously as $\Delta T \rightarrow 0$, $F_s(T) \rightarrow \delta^+(1-T)$. The numerical values of $(\Delta T)_{\text{NP}}$ at $E_{\perp} = 10 \text{ GeV}$ is $(\Delta T)_{\text{NP}} \simeq 0.16$ and at $E_{\perp} = 20 \text{ GeV}$, $(\Delta T)_{\text{NP}} \simeq 0.10$. Alternatively, we have introduced x and Q^2 independent, factorizable gaussian k_{\perp}^2 behaviour into the parton wave functions with $\langle k_{\perp}^2 \rangle \simeq (500 \text{ MeV})^2$ and we have applied the jet development Monte Carlo program of Feynman and Field [4] for the fragmentation of the final jets. Such a smearing appears necessary in the discussion of the “two-peak” structure of the experimental π^0 - π^0 azimuthal angle correlation data [43] at relatively small transverse energies ($E_{\perp} = 8-12 \text{ GeV}$, see figs. 10,11).

In some other applications (see figs. 11,12) we applied gaussian smearing together with the naive fragmentation functions (see subsect. 3.3). We would like to remark that effects given by transverse momentum smearing are not important at higher energies or in the estimate of the contribution of the $2 \rightarrow 3$ subprocesses.

In order to have sizable 3-jet effects, kinematical cuts suppressing the 2-jet contributions must be applied: e.g., one must cut the thrust variable to be smaller than a certain critical value (T_{\perp}^c) or we can require that p_{out} be larger than some reasonably chosen value. In hadron-hadron collisions, however, in contrast to e^+e^- annihilation, the relative rate of the 3-jet *versus* 2-jet contributions can also be drastically changed with energy and/or polar angle cuts and not only with cuts requiring 3-jet configurations [see eqs. (2.8), (2.9)], since the pointlike parton cross sections are folded with steeply changing parton distribution functions. We have found, e.g., that applying only transverse momentum (or jet energy) and azimuthal angle cuts, the ratio of the 3-jet/2-jet contributions ($r = \Delta\sigma(3\text{-jet})/\Delta\sigma(2\text{-jet})$) in integrated cross sections is suppressed by some large factor 3–10, as compared with the ratio of the corresponding parton cross sections* ($r_0 = \Delta\sigma_0(3\text{-jet})/\Delta\sigma_0(2\text{-jet})$). To the

* The comparison of r with r_0 depends on the incoming energy. However, with a given hadron energy \sqrt{s} we can always associate some effective parton energy range $\sqrt{\hat{s}} = \sqrt{x_a x_b s}$ in which the physical cross section obtains the dominant contribution, with the applied cuts.

Table 4
Contributions of seven different QCD $2 \rightarrow 3$ subprocesses to 3-jet production in proton-proton collisions at energy $\sqrt{s} = 52$ GeV, with azimuthal angles $\phi_i < \frac{7}{8}\pi$.

$qq' \rightarrow qq'g$ (nb)	$q\bar{q}' \rightarrow q\bar{q}'g$ (nb)	$q\bar{q} \rightarrow q\bar{q}g$ (nb)	$gq \rightarrow q'\bar{q}'q$ (nb)	$gq \rightarrow gqg$ (nb)	$g\bar{g} \rightarrow gq\bar{q}$ (nb)	$q\bar{q} \rightarrow ggg$ (nb)	p_{\perp} cut (GeV)	Transverse energy (GeV) E_{\perp}
1900 (2370)	320 (580)	14 (42)	260	3360 (5600)	120 (68)	9.4 (35)	1.5	$8 < E_{\perp} < 10$
255	40	1.5	24	380	12	0.87	2.5	$8 < E_{\perp} < 10$
490 (620)	50 (110)	2.4 (8.5)	37	540 (1090)	14 (10)	1.5 (6.8)	1.5	$10 < E_{\perp} < 12$
200	26	1.3	20	270	7.3	0.8	2.5	$10 < E_{\perp} < 12$

The values in parentheses are the cross section values of the contribution of the corresponding $2 \rightarrow 2$ subprocesses with the same value of transverse energy.

contrary, if the cross sections are calculated at (approximately) fixed transverse energy (see tables 3.4) with some relatively smaller p_{\perp} cut and a reasonable azimuthal cut (to avoid contributions from mass singularities), the value of r becomes enhanced with respect to the value of r_0 . This is a simple kinematical effect. If all the final particles were produced in the transverse momentum plane [$\theta_i = \frac{1}{2}\pi$, see eq. (2.8)], then obviously at fixed E_{\perp} the ratios r and r_0 would be the same. (If E_{\perp} were not fixed, the back-to-back configurations would be enhanced [26]). However, if we consider cross sections integrated over some finite polar angle range ($\pi - \theta_c > \theta_i > \theta_c$), then at fixed transverse energy, the effective τ -value ($\tau = x_a x_b$) of the 3-jet contribution is smaller than the effective τ -value of the 2-jet contributions. Therefore, the 3-jet contributions increase with decreasing polar angle cut θ_c . The importance of fixing the transverse energy has been realized in the ISR experiment [43].

4. Results, discussions

Similarly to the case of 2-jet effects, 3-jet contributions might be investigated by considering either direct jet effects (independent from the jet fragmentation) or various two- and three-particle correlations in the final states of the large transverse momentum particles.

Study of the transverse thrust distribution [see eq. (3.14)] appears to us to be a very convenient and totally feasible method for future analysis of the large transverse momentum particle production in high-energy hadron-hadron collisions at ISR, SPS $p\bar{p}$ collider and Isabelle energies. It provides an overall measure of the “jetness” of the process and is independent of the ambiguities of jet fragmentation.

In figs. 7a, b we have plotted the transverse thrust distributions for proton-proton collisions at $\sqrt{s} = 52$ GeV with transverse momentum cut (for jets) $p_{\perp} > 1.5$ GeV/ c and transverse energies $E_{\perp} = 8-10$ GeV and $10-12$ GeV, respectively. No polar angle cut has been applied. Except if it is not specified otherwise, in what follows, for all the figures, Q^2 dependent parton wave functions [see subsect. 3.1, parametrization (i)] have been used. We can see that the dominant subprocess is $gq \rightarrow ggq$, similarly to the $2 \rightarrow 2$ subprocesses where the largest contribution is given by gluon-quark scattering. In the same figures we have plotted the smeared 2-jet contributions, using the smearing procedure described in subsect. 3.4. It is clear that in the given kinematical regions, the smeared gaussian distribution of the $2 \rightarrow 2$ subprocesses is the dominant one throughout the entire region of the transverse thrust variable; therefore, to reveal any significant 3-jet signal appears to be very difficult. This has been expected, since even in e^+e^- annihilation, where we do not have the complications given by the bound-state wave functions, it appears very difficult to find any significant three-jet effects at $\sqrt{s} = 10-12$ GeV. In hadron collisions at these energies with $p_{\perp} > 15$ GeV/ c , contributions given by the CIM model and the background of the beam fragments might still be non-negligible. This conclusion is further confirmed by the analysis of the azimuthal correlations of $\pi^0-\pi^0$ (see figs. 10, 11).

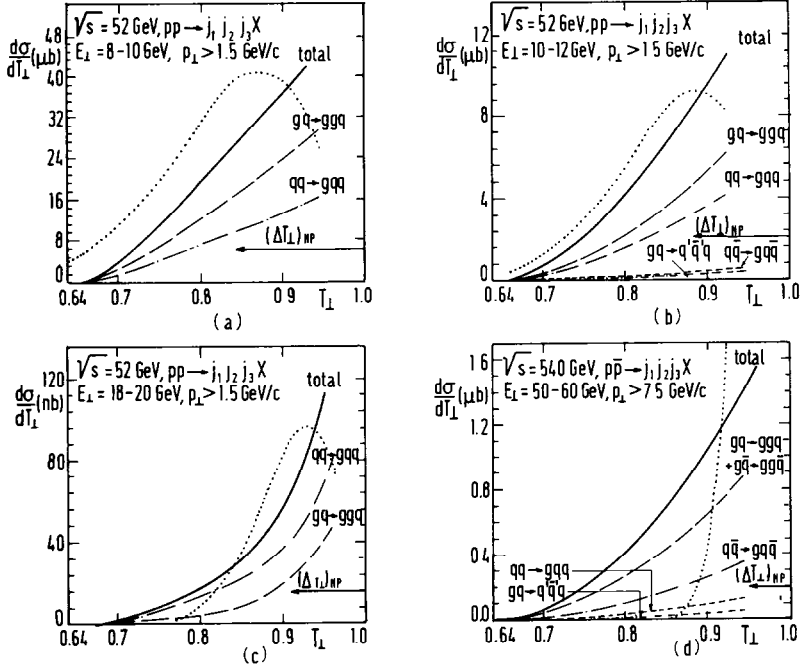


Fig. 7. $d\sigma/dT_{\perp}$ plotted for various values of E_{\perp} at (a–c) $\sqrt{s} = 52 \text{ GeV}$ and (d) $\sqrt{s} = 540 \text{ GeV}$. The contributions of different subprocesses are also indicated. The dotted curves correspond to the non-perturbative two-jet contribution calculated by smearing, described in subsect. 3.4.

Increasing the transverse energy up to $E_{\perp} = 18-20 \text{ GeV}$ (see fig. 7c) the quark-quark scattering contribution becomes dominant and the tail of the thrust distribution ($T_{\perp} < 0.75$) starts to emerge above the gaussian tail of the smeared 2-jet contribution. Although the cross section is smaller by almost three orders of magnitude, the experimental investigation of this region still appears feasible. Possible non-QCD mechanisms might be further suppressed by increasing the transverse momentum cut-off*.

We find the prediction for $p\bar{p}$ scattering at $\sqrt{s} = 540 \text{ GeV}$ particularly interesting. Requiring a cut-off $p_{\perp} > 7.5 \text{ GeV}/c$ (which might be realized by requiring a cut-off on the particles $p^{\text{particle}} > 1.0 \text{ GeV}/c$ or so) and $E_{\perp} = 50-60 \text{ GeV}$, we have obtained the thrust distribution plotted in fig. 7d. Again, the dominant subprocess is $gq \rightarrow gq\bar{q}$. For thrust values $T_{\perp} < 0.80$, the integrated cross section $\Delta\sigma \sim 0.05-0.1 \mu\text{b}$, so it can be measured at luminosities designed at the SPS proton-antiproton collider.

* We remark, that with the cuts $T_{\perp} < 0.95$ at $E_{\perp} = 20 \text{ GeV}$ the cross section decreased only $\approx 20\%$, increasing the p_{\perp} cut to $2.5 \text{ GeV}/c$. This can easily be explained by kinematical considerations. Three-jet configurations are guaranteed by the cut $T_{\perp} < 0.90$.

In the region $T_{\perp} < 0.8$, the value of the gaussian tail of the smeared 2-jet contribution is under the 3-jet tail by 1–2 orders of magnitude. We would like to emphasize that such a significant 3-jet signature is a non-trivial result, which, however, is a direct consequence of the cuts applied: with fixed transverse energy and $T_{\perp} < 0.8$, the 2-jet contributions are strongly suppressed. So we expect, that at the $p\bar{p}$ collider, in addition to the clear experimental proof of the existence of the large transverse momentum back-to-back jets (with pictures similar to the ones obtained at PETRA, at $E_{\text{cm}} = 27$ GeV, e.g. [44]) it will be feasible to find some signatures of QCD 3-jet contributions as well*. We remember (see tables 3,4) that the 3-jet/2-jet ratio decreases with increase of the polar angle cut, which may serve as a consistency check on the 3-jet interpretation.

In order to see the effects of the ambiguities given by the parameterization of the parton wave function, we have repeated the calculation of the thrust distributions corresponding to figs. 7b, d with Q^2 independent distribution functions and with the gluon wave function given by eq. (3.5). (See figs. 8a, b.) The normalizations of the contributions both of the $2 \rightarrow 2$ and $2 \rightarrow 3$ subprocesses have increased by a factor of 4–5 and the relative importance of the subprocess $gq \rightarrow ggq$ is further enhanced. The shapes of the thrust distributions have been changed only slightly. These two-gluon distributions represent the extreme parametrizations. So our predictions for the magnitudes of the cross sections presented in figs. 7a–d may be an underestimate, and the relative importance of the $2 \rightarrow 2$ and $2 \rightarrow 3$ subprocesses in the region $T_{\perp} < 0.9$ may also be somewhat different. However, our qualitative conclusion concerning the realistic feasibility of some 3-jet signatures appears to be stable against such variations of the parton wave functions.

Let us consider now the azimuthal correlations of two large transverse momentum π^0 - π^0 . Data are available from ISR experiments for transverse energies [43] 6–20 GeV.

The data are plotted for π^0 's of transverse momenta $p_{\perp} > 1.2$ GeV/c and for azimuthal difference $23^{\circ} \leq \Delta\phi < 180^{\circ}$, in transverse energy bins $E_{\perp} = 6-8, 8-10, 10-12, 12-14$ and $18-20$ (GeV). They have the characteristic feature having a “same side” ($\Delta\phi = 20^{\circ}$) and an “opposite side” enhancement ($\Delta\phi = 160^{\circ}$). Increasing the transverse energy up to $E_{\perp} = 18-20$ GeV, the broad same side peak is gradually suppressed and the opposite side peak becomes more pronounced (see fig. 11).

As to the QCD predictions, their main features can be understood without fragmenting the jets into pions. For this purpose let us discuss first the “averaged”

* A non-gaussian transverse thrust distribution may be explained by many other mechanisms not only by the 3-jet production. Therefore, its study will provide us only with a consistency check on the predicted QCD 3-jet contributions. QCD 3-jet effects can be studied at ISABELLE more quantitatively. However, at present we feel that it is premature to give any detailed predictions for this energy region.

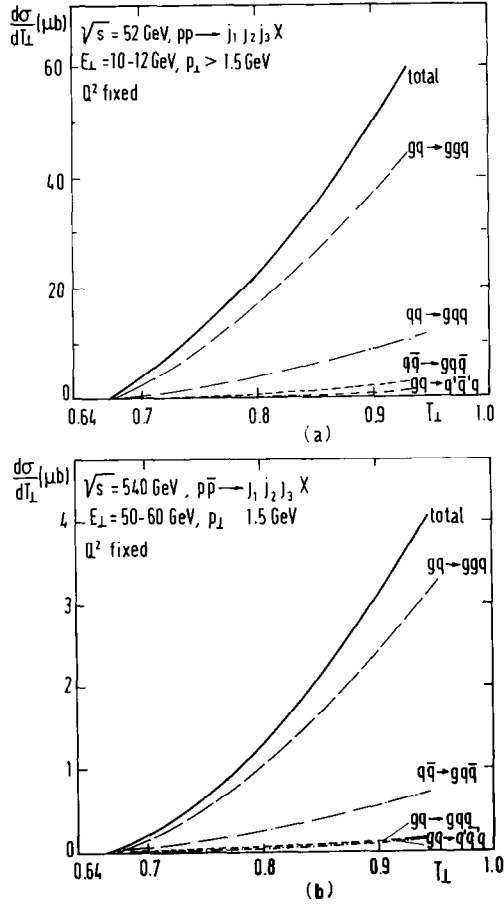


Fig. 8. (a, b) $d\sigma/dT_{\perp}$ distributions, corresponding to the curves of figs. 7b, d, respectively, are calculated by use of Q^2 independent quark wave functions [$Q^2 = Q_0^2 = 1.8 \text{ (GeV/c)}^2$] and gluon distribution given by eq. (3.5).

acoplanarity angle distributions defined as

$$\frac{d\sigma}{d\psi} = \frac{1}{3} \left(\frac{d\sigma}{d\psi_{12}} + \frac{d\sigma}{d\psi_{23}} + \frac{d\sigma}{d\psi_{31}} \right), \quad (4.1)$$

where $\psi_{ij} = \pi - \phi_{ij}$ and ϕ_{ij} denotes the azimuthal angle difference for any two of the final jets*. For transverse energy values $E_{\perp} = 8-20 \text{ GeV}$, which transverse

* Whether or not we include the statistical factors in the differential cross sections of identical particles in the final state is a matter of convention. Since we must add different subprocesses, it appears to us to be more natural to include them. In the calculation of integrated cross sections, however, they must be included.

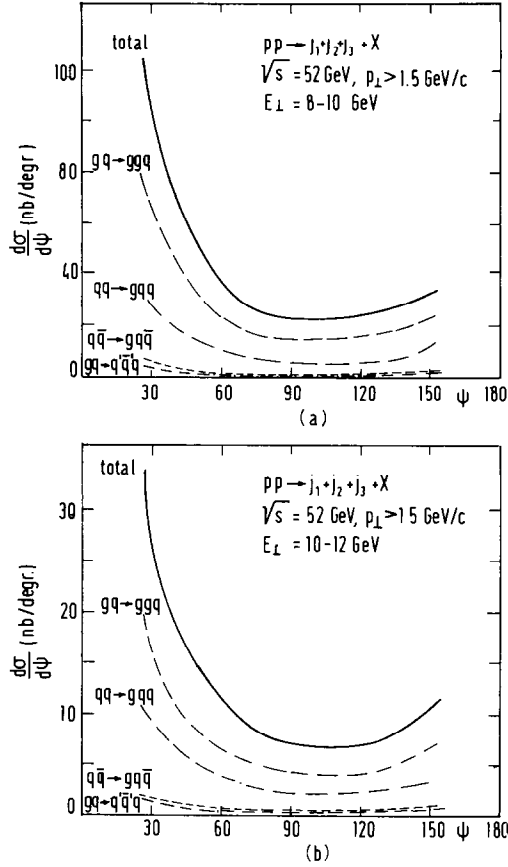


Fig. 9. (a, b) Acoplanarity angle distributions of jets produced in pp collisions at $\sqrt{s} = 52$ GeV. Polar angle cuts $45^\circ < \theta_i < 135^\circ$ have been used. The cross-section values have been calculated by averaging over the three possible pairings of the final jets [see eq. (4.1)].

momentum cut $p_{\perp} > 1.5$ GeV/c in the azimuthal region the infrared-singular parts of the $2 \rightarrow 3$ subprocesses cannot contribute.

In figs. 9a,b we have plotted the acoplanarity distributions [average over ψ_{ij} , see eqs. (2.3) and (4.1)] for three-jet production in proton-proton collisions at $\sqrt{s} = 52$ GeV at two transverse energy bins $E_{\perp} = 8-10$ GeV and $10-12$ GeV, respectively, with transverse momentum cut $p_{\perp}^{\text{jet}} > 1.5$ GeV/c and polar angle cut $45^\circ < \theta < 135^\circ$ [see eq. (2.2)]. The curves have the characteristic shape of acoplanarity distribution of Bhabha scattering (in the same angular region). The opposite side peak (ψ is small) survives the cuts, however, the same side peak (ψ is near to 180°) is indicated only by the presence of a slight increase above $\psi \approx 120^\circ$. We remark that, in general, the shape of the acoplanarity distribution should not be symmetric

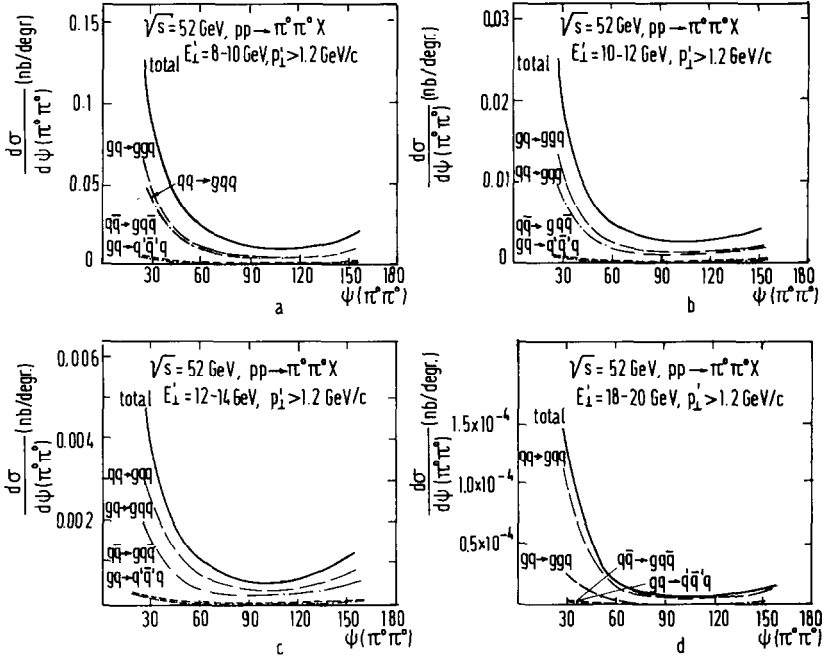


Fig. 10. (a–d) Acoplanarity angle distributions of $\pi^0\pi^0$ pairs produced in pp collisions at $\sqrt{s} = 52$ GeV. The prime for E_{\perp}' and p_{\perp}' indicates that the cut-offs have been applied to the three-momenta of the final pions. The cross-section values have been calculated by polar angle cuts $45^\circ < \theta_i < 135^\circ$. (We remember that the azimuthal angle is $\phi = \pi - \psi$.)

around $\psi = 90^\circ$ since there is no $\psi \leftrightarrow \pi - \psi$ symmetry in the azimuthal difference. The shape of the curves does not change qualitatively with increasing E_{\perp}' ; however, its normalization decreases sharply. We remark, that the curves obtained for the contributions of the subprocess $qq \rightarrow gq$ are in agreement with the calculations of Kripfganz and Schiller [26], as far as the comparison is possible.

In figs. 10a, b we have plotted the acoplanarity distributions for $\pi^0\pi^0$ production. In this case all the kinematical variables are defined in terms of the momenta of the final pions. For the fragmentation functions we used the naive Q^2 independent functions, described in subsect. 3.2.

Comparing figs. 10a, b and 9a, b, we can see that due to the softer gluon fragmentation function, the relative magnitude of the subprocess $gq \rightarrow ggq$ has been decreased, although it is still dominant. The shape of the curves has changed only slightly, while their normalizations have been decreased by approximately three orders of magnitude. In figs. 10c, d we have also plotted the distributions at transverse energies $E = 12\text{--}14$ GeV and $18\text{--}20$ GeV. With increasing E_{\perp}' the normalization decreases approximately like the p_{\perp} behaviour of the inclusive π^0 production cross section and the quark-quark scattering contributions become more and more dominant, but the

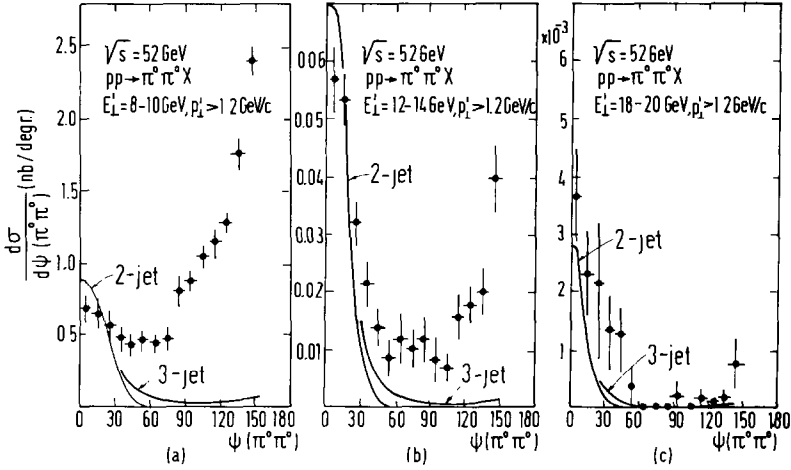


Fig. 11. (a–c) Acoplanarity angle distributions of smeared 2-jet and 3-jet contributions. The data points [43] have been normalized to the $\psi = 0$ peak of the 2-jet contributions of (b). The smearing procedure (width parameters and method of regularization) is described in sect. 4. The kinematical cuts are the same as for fig. 10.

shape of the curves remains qualitatively the same. Finally we remark that the ratio of the 3-jet/2-jet contributions becomes smaller with jet fragmentation into π^0 's (figs. 10) than without fragmentation (it is $\approx 25\%$ with the applied cuts).

Especially at the smallest E_{\perp} values, the theoretical acoplanarity distributions of figs. 10a–d are very different from the measured distributions, plotted in figs. 11a–c. The QCD contributions do not explain the spectacular suppression of the same side peak, obtained with the increase of the transverse energy E_{\perp} . Nor can it be explained by the smeared 2-jet contributions since in this case the width of the same side enhancement must be smaller than the opposite side peak. The same side contributions are completely given by jet broadening, while the back-to-back peak also receives contributions from the initial state smearing. We have checked this with an explicit calculation using the Feynman and Field Monte Carlo jet development model [46] to smear the contribution of the $2 \rightarrow 2$ subprocesses. We have found that in addition to the expected narrower shape of the same side contributions, the opposite side peak is also too sharp. Using for the transverse momentum smearing in the initial state and in the final jets gaussian distributions $\langle q_{\perp}^2 \rangle = 2(0.5 \text{ GeV}/c)^2$ and $\langle q'_{\perp}{}^2 \rangle = 2(0.3 \text{ GeV}/c)^2$, respectively, the obtained peaks at $\psi = 0$ are much narrower than the experimental distributions. In order to fit the enhancement at $\psi = 0$ we used larger values $\langle q_{\perp}^2 \rangle = 2(0.6 \text{ GeV}/c)^2$ and $\langle q'_{\perp}{}^2 \rangle = 2(0.45 \text{ GeV}/c)^2$, respectively*.

* We required that the angles between the two final partons and the angles between the beam axis and the final partons be larger than 0.25 rad (δ -cut) and the initial parton energy $\sqrt{\hat{s}} > 4 \text{ GeV}$ (see table 1), in the parton c.m. system. The singular contributions from the very small \hat{t} , \hat{u} or \hat{s} regions can not contribute. With this "regularization" of the smearing the integrated cross section changed negligibly with the given increase of $\langle q_{\perp}^2 \rangle$ and $\langle q'_{\perp}{}^2 \rangle$.

The 2-jet contributions obtained by this smearing are plotted in figs. 11a–c, where the smeared 3-jet contributions \star are also given (their normalization is fixed by fitting the data at $E_{\perp} = 12\text{--}14$ GeV near $\psi = 0$ with the 2-jet contributions). As we can see, to fit the measured distributions by 3-jet contributions [26] appears to be unjustified.

An explanation for this is provided by noticing that the transverse momentum cut used for the experimental acoplanarity distributions is dangerously small ($p_{\perp} > 1.2$ GeV/c).

Large contributions might still be given by the reaction where one of the π^0 's belongs to the beam particle fragments. For smaller transverse energy bins ($E_{\perp} = 8\text{--}10$ GeV), these contributions are much larger for the same side configurations ($\psi = \pi$), than at $\psi = 0$. They become, however, more isotropic as E_{\perp} increases. Indeed, the main characteristics of the behaviour of the same side peak of the measured distributions can be quantitatively interpreted in terms of this background [45].

However, increasing the transverse momentum cut the QCD contributions decrease according to some power law (see first footnote of this section) while the background drops exponentially. Therefore we expect that at larger values of the p_{\perp} cut, the same side enhancement ($\psi = \pi$) must disappear and the opposite side peak ($\psi = 0$) must become sharper, as predicted by the QCD model.

The p_{out} distributions of π^0 - π^0 correlations have also been analysed [43]. As it has been pointed out in ref. [21], the broad shape of the measured p_{out} distributions cannot be explained by smeared 2-jet contributions. It is expected, however, that similarly to the transverse momentum distribution of the massive $\mu^+\mu^-$ pairs of the Drell–Yan process, the large momentum tails of the p_{out} distributions are correctly described by 3-jet contributions. At transverse momentum values of the trigger pion $p_{\perp} = 5$ GeV/c and x_e values $x_e \approx 0.4\text{--}0.5$, the background contributions discussed above are suppressed. So, in this case we have better justification to fit the tail of the experimental distributions by the smeared 3-jet contributions. The result is plotted in figs. 12a–c, where the data points have been normalized to the theoretical value at $p_{\text{out}} = 1$ GeV/c for the curve with $5 < p_{\perp} < 6$, $0.6 < x_e < 0.8$. The agreement between the nine theoretical curves and the experiment, both in shape and normalization, is remarkably good. We notice that better agreement could be obtained for the normalization by modifying the fragmentation functions $D_{\pi^0}^{\pi^0}(z)$ (e.g., introducing Q^2 dependence, as predicted by QCD). The smearing in the kinematical region of the figs. 12a–c is still important. The theoretical curves without smearing are steeper. The shape of the p_{out} distributions becomes independent of smearing only above $p_{\text{out}} \simeq 3\text{--}4$ GeV/c.

\star The smeared 3-jet contributions have been calculated by ϵ and δ cuts (see sect. 2) $\epsilon = 0.1$, $\delta = 0.25$, applied to the momenta of the final partons in the parton c.m. systems, with $\langle q_{\perp}^2 \rangle = 2(0.5 \text{ GeV}/c)^2$ and $\langle q_{\perp}^{\prime 2} \rangle = 2(0.35 \text{ GeV}/c)^2$.

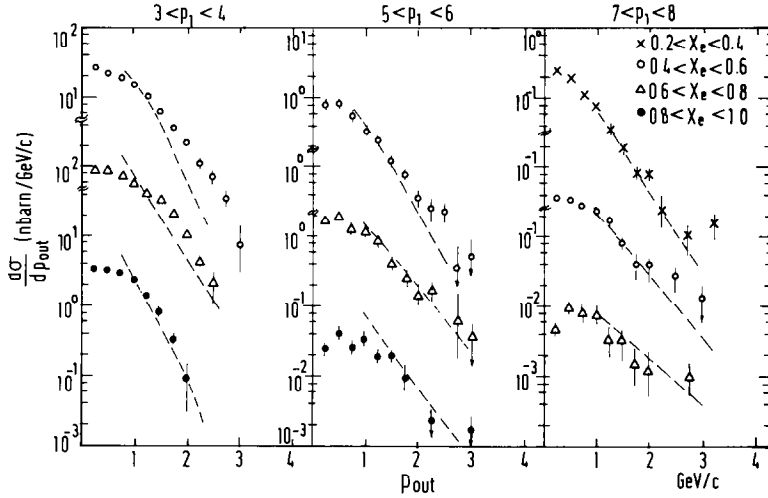


Fig. 12. p_{out} distributions at various trigger particle transverse momentum $p_{\perp} = |\mathbf{p}_{\perp \text{trigger}}|$ and x_e bins (see fig. 5). It has been required that $p_{\perp} \geq |\mathbf{p}_{\perp \text{away}}|$ and polar angle cut $45^\circ < \theta_i < 135^\circ$ has been used. The smeared 3-jet contributions are plotted by dashed lines. The data points [43] have been normalized to the second curve of b (at $p_{\text{out}} \approx 1.0$ GeV/c). The smearing procedure is described in sect. 4.

5. Conclusions

Two or more particle correlations or jet correlations in the production of large transverse momentum particles in hadron-hadron collisions must be dominated by the contributions of $2 \rightarrow 3$ QCD subprocesses in various kinematical regions. The main contributions to physical cross sections at the ISR energies (depending on the value of the transverse energy) are given by the processes $gq \rightarrow gqq$ and $qq \rightarrow gqq$. The annihilation reactions (like $q\bar{q} \rightarrow ggg$), are, in general, negligible. At even higher energies ($p\bar{p}$ collider, ISABELLE) the process $gg \rightarrow ggg$ will be important. The normalization and the relative importance of the various subprocesses still depends sensitively on the poorly known gluon distribution and fragmentation functions, but the shapes and slopes of the distributions are less affected, because the dominant subprocesses behave similarly.

We have shown by a quantitative comparison of the presently available correlation data and the predictions of the QCD model based on the $2 \rightarrow 3$ subprocesses that the measured distributions are still biased by background contributions and transverse momentum smearing. The shape of the p_{out} distributions, however, can be described by the smeared 3-jet contributions.

We have pointed out that in case of 3-jet production in hadron-hadron collisions, cuts imposed on polar angles, energy and momentum variables may also change the

3-jet/2-jet ratio significantly (in addition to the geometrical cuts like cuts on the azimuthal angle, p_{out} or transverse thrust values). In order to find clear 3-jet effects, independent of transverse momentum smearing and background contributions, we propose to impose a transverse momentum cut of at least $p_{\perp} > 2.0 \text{ GeV}/c$ for each particle and to plot the correlations at approximately fixed transverse energies above $E_{\perp} \approx 15\text{--}20 \text{ GeV}$. The values of the corresponding integrated cross sections are large enough to obtain significant 3-jet signals in future experiments at ISR, SPS $p\bar{p}$ collider and ISABELLE. The experimental confirmation of the predicted 3-jet effects would provide us with very important tests on the QCD model proposed for the description of large transverse momentum production in hadron-hadron collisions.

We are grateful to J. Gunion and E. Reya for valuable discussions. One of us (Z.K.) thanks D. Lissauer for his helpful correspondence concerning the ISR data. We also thank DESY for hospitality. E.P. gratefully acknowledges the support by the Academy of Finland.

Appendix

In the case of 2q-2q-1g subprocesses we can specify the process (2.1) to be quark-antiquark annihilation

$$q(-p_4) + \bar{q}(-p_5) \rightarrow \bar{q}'(p_1) + q'(p_2) + g(p_3). \quad (\text{A.1})$$

The cross section and the definition of the kinematics remain the same as given by eqs. (2.1)–(2.5) in terms of the four-vectors

$$x_{ij} = (p_i + p_j)^2, \quad s_{ij} = x_{ij}.$$

The factor C has the value $C = \frac{1}{36}$. For this process $N_a = 5$ [see eq. (2.5)], since we have only 5 Feynman diagrams, as given in fig. 2a. The color matrix has the form ^{*}

$$C^{(a)} = -\frac{16}{3} \times \begin{bmatrix} 8 & 1 & 9 & -2 & -7 \\ 0 & 8 & 9 & -7 & -2 \\ 0 & 0 & 18 & -9 & -9 \\ 0 & 0 & 0 & 8 & 1 \\ 0 & 0 & 0 & 0 & 8 \end{bmatrix}. \quad (\text{A.2})$$

The matrix elements of the Lorentz matrix $A^{(a)}(s_{ij})$ have the expressions

$$\begin{aligned} A(1, 1) &= -(s_{42}s_{53} + s_{43}s_{52})/(s_{31}s_{54}^2); \\ A(1, 2) &= \{s_{12}[s_{41}(2s_{52} + s_{53}) + s_{42}(2s_{51} + s_{53}) + s_{43}(s_{51} + s_{52})] \\ &\quad + s_{23}[s_{41}(-2s_{51} + s_{52}) + s_{42}s_{51}]\} \end{aligned}$$

* The factor (-16) appearing here is an overall factor for the Lorentz part of the amplitude.

$$\begin{aligned}
& + s_{31} [s_{41}s_{52} + s_{42}(s_{51} - 2s_{52})] \} / (2s_{23}s_{31}s_{54}^2) ; \\
A(1, 3) = & \{s_{12} [-2s_{31}s_{54} + s_{41}(4s_{52} + 3s_{53}) + s_{42}(4s_{51} + 3s_{53}) \\
& + s_{43}(3s_{51} + 3s_{52} + 2s_{53})] + s_{23} [s_{41}(-6s_{51} + s_{52} - s_{53}) \\
& + (s_{42} - s_{43})s_{51}] + s_{31} [(s_{41} - 3s_{43})s_{52} \\
& + s_{42}(s_{51} - 2s_{52} - 3s_{53})] \} / (4s_{12}s_{13}s_{54}^2) ; \\
A(1, 4) = & \{s_{51} [-s_{12}s_{43} + s_{23}s_{41} + s_{42}s_{43}] + s_{31} [(2s_{41} + 2s_{43})s_{52} \\
& + s_{42}(s_{51} - s_{54})] + s_{41} [2(s_{41} + s_{43})s_{52} \\
& + s_{42}(2s_{51} + s_{53})] \} / (2s_{12}s_{31}s_{43}s_{54}) ; \\
A(1, 5) = & A(1, 4)[4 \leftrightarrow 5]; \quad A(2, 2) = A(1, 1)[1 \leftrightarrow 2]; \\
A(2, 3) = & A(1, 3)[2 \leftrightarrow 1]; \quad A(2, 4) = A(1, 4)[1 \leftrightarrow 2]; \\
A(2, 5) = & A(2, 4)[4 \leftrightarrow 5]; \\
A(3, 3) = & \{s_{12} [2s_{54}(s_{12} - s_{23} - s_{31}) + s_{41}(-2s_{51} + 6s_{52} + 5s_{53}) \\
& + s_{42}(6s_{51} - 2s_{52} + 5s_{53}) + s_{43}(5s_{51} + 5s_{52} + 4s_{53}) \\
& + s_{23} [-2s_{31}s_{54} + s_{41}(-6s_{51} + s_{52} - 3s_{53}) + (s_{42} - 3s_{43})s_{51}] \\
& + s_{31} [(s_{41} - 3s_{43})s_{52} + s_{42}(s_{51} - 6s_{52} - 3s_{53})] \} / (4s_{12}^2s_{54}^2) ; \\
A(3, 4) = & \{s_{12} [s_{54}(s_{23} + s_{31} + s_{41} + s_{42}) - 2s_{43}(s_{51} + s_{52})] \\
& + s_{23} [s_{54}(2s_{31} - s_{41}) + s_{41}(s_{52} - s_{53}) + 3(s_{42} + s_{43})s_{51}] \\
& + s_{31} [3(s_{41} + s_{43})s_{52} + s_{42}(s_{51} - s_{53} - s_{54})] \\
& + s_{41}s_{52}(3s_{41} + s_{42} + 3s_{43}) + s_{42}s_{51}(s_{41} + 3s_{42} + 3s_{43}) \\
& + 2s_{41}s_{42}s_{53} \} / (4s_{12}^2s_{43}s_{54}) ; \tag{A.3} \\
A(3, 5) = & A(3, 4)[4 \leftrightarrow 5]; \quad A(4, 4) = A(1, 1)[4 \leftrightarrow 1, 5 \leftrightarrow 2]; \\
A(4, 5) = & A(1, 2)[4 \leftrightarrow 1, 5 \leftrightarrow 2]; \quad A(5, 5) = A(4, 4)[4 \leftrightarrow 5].
\end{aligned}$$

The cross section of the crossed subprocess

$$q(-p_4) + g(-p_5) \rightarrow \bar{q}'(p_1) + q'(p_2) + q(p_3) \tag{A.4}$$

is obtained by crossing g with \bar{q} ; therefore,

$$k_i = p_i \quad \text{if } i = 1, 2, 4, \quad k_3 = p_5, \quad k_5 = p_3,$$

and the invariant variables s_{ij} have the same expressions in terms of k_i, k_j as before ($s_{ij} = 2k_i k_j$).

The kinematical variables, $q^2, |t|, d\Omega^{YT}$, however, [see eqs. (2.2), (2.3a) and (2.4)] are defined in terms of the variables p_i :

$$q^2 = (p_1 + p_2)^2, \quad t = (p_4 + q)^2, \quad s = (p_4 + p_5)^2$$

$$\cos \theta^{\text{TY}} = - \frac{\mathbf{p}_2 \mathbf{p}_2}{|\mathbf{p}_2| |\mathbf{p}_5|} \Big|_{\mathbf{q}=0}, \quad \cos \phi^{\text{TY}} = - \frac{(\mathbf{p}_2 \times \mathbf{p}_5)(\mathbf{p}_3 \times \mathbf{p}_5)}{|\mathbf{p}_2 \times \mathbf{p}_5| |\mathbf{p}_3 \times \mathbf{p}_5|} \Big|_{\mathbf{q}=0}.$$

For the process (A.4) the color factor is negative $C = -\frac{1}{96}$.

Note added in proof

Planar hadronic events, predicted by 3-jet production in e^+e^- annihilation have been found at PETRA, DESY, in all the four experiments. After submitting this work for publication we received a paper by T. Gottschalk and D. Sivers (to be published in Phys. Rev. D) in which calculation of the spin and colour averaged invariant matrix elements have been reported for all the $2 \rightarrow 3$ QCD subprocesses. We compared the computer programs obtained for the invariant matrix element numerically and found complete agreement. We are grateful to these authors for sending us their computer program.

References

- [1] M. Banner et al., Phys. Lett. 41B (1972) 547; 44B (1973) 537;
F.W. Büsser et al., Phys. Lett. 46B (1973) 471; 51B (1974) 306; 55B (1975) 233;
M. Jacob, P.V. Landshoff, Phys. Reports 48 (1978) 285.
- [2] S.M. Berman, J.D. Bjorken and J.B. Kogut, Phys. Rev. D4 (1971) 3388;
S.D. Ellis and M. Kislinger, Phys. Rev. D9 (1974) 2027.
- [3] D. Sivers, R. Blankenbecler and S.J. Brodsky, Phys. Reports 23 (1976) 1.
- [4] R.P. Feynman, R.D. Field and G.C. Fox, Nucl. Phys. B128 (1977) 1.
- [5] B.L. Combridge, J. Kripfganz and J. Ranft, Phys. Lett. 70B (1977) 234;
R. Cutler and D. Sivers, Phys. Rev. D17 (1978) 196.
- [6] H.D. Politzer, Phys. Lett. 70B (1977) 430;
A.H. Mueller, Columbia Univ. preprint CU-TP-125 (1978);
C.T. Sachrajda, Phys. Lett. 76B (1978) 100;
R.K. Ellis, H. Georgi, M. Machacek, H.D. Politzer and G.G. Ross, Nucl. Phys. B152 (1979) 285;
Yu.L. Dokshitzer, D.I. Dyakonov and S.I. Troyan, Leningrad preprint and Proc. 13th Leningrad Winter School (1978) (in English SLAC Trans-183);
D. Amati, R. Petronzio and G. Veneziano, CERN TH 2527 (1978);
W. Furmanski, Cracow Univ. Preprint TPJU 10/78;
J. Kripfganz, Leipzig preprint, KMU-HEP-78-12 (1978).
- [7] G. Anderson et al., Phys. Rev. Lett. 41 (1978) 616;
J.G.H. De Groot et al., QCD analysis of charged current structure function, Univ. Dortmund preprint 12/78 (1978);
P.C. Bosetti et al., Nucl. Phys. B142 (1978) 1.
- [8] G. Altarelli, G. Parisi and R. Petronzio, Phys. Lett. 76B (1978) 351, 356.
- [9] H. Fritzsch and P. Minkowski, Phys. Lett. 73B (1978) 80.
- [10] K. Kajantie and R. Raitio, Nucl. Phys. B139 (1978) 72.
- [11] K. Kajantie, J. Lindfors and R. Raitio, Helsinki report HU-TFT-78-18;
K. Kajantie and J. Lindfors, Helsinki report HU-TFT-78-33.
- [12] C. Michel and T. Weiler, Contribution to 13th Rencontre de Moriond, Les Arcs, France (1978).

- [13] F. Halszen and D. Scott, Phys. Rev. Lett. 40 (1978) 1117.
- [14] Z. Kunszt, E. Pietarinen and F. Reya, DESY preprint DESY 79/28 (1979), Phys. Rev. D, to be published.
- [15] S.W. Herb et al., Phys. Rev. Lett. 39 (1977) 252;
W.R. Innes et al., Phys. Rev. Lett. 39 (1977) 1240 (E: 39 (1977) 1640);
D.M. Kaplan et al., Phys. Rev. Lett. 40 (1978) 435;
K. Ueno et al., Phys. Rev. Lett. 42 (1979) 478.
- [16] C. Kourkoumelis et al., Electron production at ISR, BNL preprint BNL-25075 (1979);
J.G. Branson et al., Phys. Rev. Lett. 38 (1977) 1331.
- [17] M. Della Negra et al., CCHK Collaboration, Nucl. Phys. B127 (1977) 1.
- [18] R.D. Field, Talk at 19th Int. Conf. on High-energy physics, Tokyo, 1978, CALT-68-683 (1978).
- [19] H. Meyer, talk at Nordita Meeting, Copenhagen, April, 1979.
- [20] R. Baier, J. Cleymans, K. Kinoshita and B. Peterson, Nucl. Phys. B118 (1977) 139.
- [21] R.D. Field, Phys. Rev. Lett. 40 (1978) 997;
R.P. Feynman, R.D. Field and G.C. Fox, Phys. Rev. D18 (1978) 3320.
- [22] A.P. Contogouris and R. Gaskell, Nucl. Phys. B126 (1977) 157.
- [23] P.V. Landshoff, Large- p_{\perp} physics, Talk presented at the ISR Workshop, 14–21 Sept. 1977, Proc. ed. M. Jacob;
J.F. Owens, E. Reya and M. Glück, Phys. Rev. D18 (1978) 1501.
- [24] R. Baier and B. Petersson, University of Bielefeld preprint, BI-TP77/08.
- [25] M.K. Chase, University of Cambridge preprint DAMPT 77/29 (1977);
M.K. Chase and W.J. Stirling, Nucl. Phys. B133 (1978) 157.
- [26] J. Kripfganz and A. Schiller, Phys. Lett. 79B (1978) 317;
C.J. Maxwell, Nucl. Phys. B, to be published.
- [27] G. Altarelli, R.K. Ellis, G. Martinelli, Nucl. Phys. B143 (1978) 521 (E: B146 (1978) 544);
B157 (1979) 461.
- [28] J. Kubar-André and F.E. Paige, Phys. Rev. D19 (1979) 221;
A.P. Contogouris and J. Kripfganz, Scale violations and the quark gluon correction to the Drell-Yan formalism, McGill preprint (1978); The quark-quark correction to the Drell-Yan formalism, McGill preprint (1979);
K. Harada, T. Kaneko and N. Sakai, Nucl. Phys. B155 (1979) 169.
- [29] Z. Kunszt and E. Pietarinen, DESY preprint 79/18 (1979).
- [30] K. Koller, Z. Kunszt and E. Pietarinen, to be published.
- [31] F.A. Behrends, K.J.F. Gaemers and R. Gastmans, Nucl. Phys. B63 (1973) 541.
- [32] G. Sterman and S. Weinberg, Phys. Rev. Lett. 39 (1977) 1436.
- [33] G. Altarelli and G. Parisi, Nucl. Phys. B126 (1977) 298.
- [34] H. Georgi, Phys. Rev. Lett. 42 (1979) 294.
- [35] A.J. Buras and K.J.F. Gaemers, Nucl. Phys. B132 (1978) 2498.
- [36] J.F. Owens and E. Reya, Phys. Rev. D17 (1978) 3003.
- [37] J.F. Owens, E. Reya and M. Glück, ref. [23].
- [38] R.D. Field and R.P. Feynman, Phys. Rev. D15 (1977) 2590.
- [39] E. Fahri, Phys. Rev. Lett. 39 (1977) 1237.
- [40] A. De Rújula, J. Ellis, E.G. Floratos and M.K. Gaillard, Nucl. Phys. B138 (1978) 387.
- [41] G.C. Fox and S. Wolfram, Phys. Lett. 82B (1979) 134; Phys. Rev. Lett. 41 (1978) 1581.
- [42] P. Binétruy and G. Girardi, Nucl. Phys. B155 (1979) 150.
- [43] C. Cobb et al., Phys. Rev. Lett. 40 (1978) 1420;
C. Kourkoumelis et al., CERN-EP/79-36 (1979).
- [44] B. Wiik, Talk at the Neutrino '79 Symp. Bergen, 1979.
- [45] J.F. Gunion, Z. Kunszt and E. Pietarinen, Phys. Rev. D, to be published.
- [46] R.D. Field and R.P. Feynman, Nucl. Phys. B136 (1978) 1;
T. Sjöstrand, B. Söderberg, Lund preprint, LUTP 78-18.